### Title

Label-Free Visualization and Quantification of Biochemical Markers of Atherosclerotic Plaque Progression Using Intravascular Fluorescence Lifetime




### Journal

JACC Cardiovascular Imaging, 14(9)

### ISSN

1936-878X



### Authors

Bec, Julien
Vela, Deborah
Phipps, Jennifer E
et al.



### Publication Date

2021-09-01

### DOI

10.1016/j.jcmg.2020.10.004

Peer reviewed

HHS Public Access

Author manuscript

*JACC Cardiovasc Imaging*. Author manuscript; available in PMC 2022 September 01.

Published in final edited form as:

*JACC Cardiovasc Imaging*. 2021 September ; 14(9): 1832–1842. doi:10.1016/j.jcmg.2020.10.004.

# Label-free visualization and quantification of biochemical markers of atherosclerotic plaque progression using intravascular fluorescence lifetime

**Julien Bec, PhD**[a], **Deborah Vela, MD**[b], **Jennifer E. Phipps, PhD**[a], **Michael Agung, MS**[a], **Jakob Unger, PhD**[a], **Kenneth B. Margulies, MD**[c], **Jeffrey A. Southard, MD**[d], **L. Maximilian Buja, MD**[b,e], **Laura Marcu, PhD**[a]

[a]Department of Biomedical Engineering, University of California, Davis, CA, USA

[b]Department of Cardiovascular Pathology Research, Texas Heart Institute, Houston, TX, USA

[c]Cardiovascular Institute, Perelman School of Medicine, University of Pennsylvania, Philadelphia, PA, USA

[d]Division of Cardiovascular Medicine, UC Davis Health System, University of California, Davis, Sacramento, CA, USA

[e]Department of Pathology and Laboratory Medicine, the University of Texas Health Science Center at Houston, Houston, TX, USA

## Abstract

**OBJECTIVES—**This study aimed to systematically investigate whether plaque autofluorescence properties assessed with intravascular fluorescence lifetime imaging (FLIm) can provide qualitative and quantitative information about intimal composition and improve the characterization of atherosclerosis lesions.

**BACKGROUND—**Despite advances in cardiovascular diagnostics, the analytical tools and imaging technologies currently available have limited capabilities for evaluating in situ biochemical changes associated with luminal surface features. Earlier studies of small number of samples have shown differences among the autofluorescence lifetime signature of well-defined lesions, but a systematic pixel-level evaluation of fluorescence signatures associated with various histological features is lacking and needed to better understand the origins of fluorescence contrast.

**METHODS—**Human coronary artery segments (n=32) were analyzed with a bimodal catheter system combining multispectral FLIm with intravascular ultrasonography, compatible with in

**ADDRESS FOR CORRESPONDENCE:** Dr. Laura Marcu, Department of Biomedical Engineering, University of California, Davis, 2513 GBSF, 451 E. Health Sciences Dr., Davis, California 95616. Tel: 530-752-0288; fax: 530-754-5739; lmarcu@ucdavis.edu.

**Disclosures:** The intravascular ultrasonography system and additional related components used for this work were provided by Boston Scientific.

vivo coronary imaging. Various histologic components present along the luminal surface (200-μm depth) were systematically tabulated (12 sectors) from each serial histological section (n=204). Morphologic information provided by ultrasonography allowed for the accurate registration of imaging data with histology data. The relationships between histologic findings and FLIm parameters obtained from three spectral channels at each measurement location (n=33,980) were characterized.

**RESULTS—**Our findings indicate that fluorescence lifetime from different spectral bands can be used to quantitatively predict the superficial presence of macrophage foam cells (mFCs) (ROC-AUC: 0.94) and extracellular lipid content in advanced lesions (lifetime increase in 540-nm band), detect superficial calcium (lifetime decrease in 450-nm band ROC-AUC: 0.90), and possibly detect lesions consistent with active plaque formation such as pathological intimal thickening and healed thrombus regions (lifetime increase in 390-nm band).

**CONCLUSIONS—**Our findings indicate that autofluorescence lifetime provides valuable information for characterizing atherosclerotic lesions in coronary arteries. Specifically, FLIm can be used to identify key phenomena linked with plaque progression (e.g., peroxidized-lipid–rich mFC accumulation and recent plaque formation).

### Keywords

Imaging; Atherosclerosis; Coronary Artery Disease; Inflammation; Lipids and Cholesterol; Ultrasonography; Percutaneous Coronary Intervention Imaging; Atherosclerosis; Coronary Artery Disease; Inflammation; Ultrasound

## INTRODUCTION

Critical coronary events have been associated with the rupture of a thin fibrotic cap, the presence of abundant inflammatory cells (primarily macrophages), and the formation of thrombus on the eroded intima (1,2). Despite advances in cardiovascular diagnostics, the analytical tools and imaging technologies currently available have limited capabilities for measuring biochemical changes at the luminal surface associated with features known to play a role in the progression and destabilization of atherosclerotic lesions (3).

Fluorescence lifetime–based techniques utilize the autofluorescence properties of endogenous molecular complexes, including lipids, lipoproteins, structural proteins (eg, elastin, collagen, proteoglycans), and their cross-links (4), to assess biochemical composition. Several studies have shown that time-resolved fluorescence spectroscopy (5,6) and, more recently, point-scanning fluorescence lifetime imaging (FLIm) (7–9) can resolve variations in biochemical compositions associated with distinct stages of plaque progression. Moreover, the suitability of FLIm for in vivo assessment of narrow coronary vessels during cardiac catheterization (10) was demonstrated by using a bimodal FLIm/intravascular ultrasonography (IVUS) catheter system and, more recently, in combination with optical coherence tomography (11).

Despite these advances, the full diagnostic potential of FLIm has not been fully explored. Although studies (7,12) have shown that autofluorescence-derived optical parameters can be related to the presence of specific molecular species (eg, collagen, elastin), distinctive cell

types (eg, macrophages), or morphologic characteristics (eg, lipid pool under a thin fibrotic cap), these studies were limited to well-defined lesions. Systematic studies linking FLIm parameters with the specific biochemical makeup of arterial plaque are lacking.

Accordingly, the primary goal of our study was to determine, at the pixel level, whether the rich spatial variation of FLIm-derived parameters observed over the luminal surface of diseased human coronary arteries is quantitatively linked to the presence of various plaque constituents. We further determined whether FLIm data could be used to better characterize atherosclerotic plaque to support the diagnosis of critical plaque pathophysiology.

## METHODS

### FLIm-IVUS Imaging System.

This system comprises a multimodal catheter, a motor drive, and a console that enable the acquisition of coregistered IVUS (40 MHz) and FLIm data at 30 frames/s. This system can be used in vivo to image coronary arteries (10). Briefly, pulsed ultraviolet laser light (355 nm) induces autofluorescence from tissues that can be separated into 4 distinct spectral bands of the instrument (390/40 nm, 450/45 nm, 540/50 nm, and 630/53 nm). A photomultiplier detects the fluorescence signal, which is then sampled with a high-speed digitizer and saved for further processing. Details are presented in the Supplemental Methods section and in Supplemental Figures 1–2.

### Specimens.

Coronary arteries were procured from patients undergoing heart transplant (n=9) and organ donors (n=23) according to protocols approved by the institutional review boards at the University of Pennsylvania and the University of California, Davis. Donor and transplant patient characteristics are shown in Supplemental Table 1.

### Imaging Procedure.

Mounted artery segments were immersed in a 37°C saline bath with luminal flushing (3 $cm^3$/s), and imaging pullbacks were performed (5 s, 20–50 mm length, 150 FLIm-IVUS cross-sectional images). The imaging depth was approximately 200 μm for FLIm and 3–4 mm for IVUS.

### FLIm-IVUS Data.

Both average fluorescence lifetime and spectral ratio values were computed for each pixel with a Laguerre basis expansion technique (13). For each FLIm parameter, *en face* maps were generated in which each pixel location corresponded to a distinct angular and axial pullback position. FLIm data were mapped onto the IVUS-derived vessel lumen to generate 3D FLIm maps and IVUS-FLIm overlay images (Supplemental Figures 2B–D and 3).

### Histology.

Serial sectioning of perfusion-fixed (10% neutral-buffered formalin) paraffin-embedded artery samples (5-μm thick, 250 μm intervals) was performed. Sections were stained with hematoxylin and eosin stain and modified Movat's pentachrome. Anti-CD68 (Dako

North America, Inc, Carpinteria, CA) and anti-α-SMC-actin (Sigma-Aldrich, St. Louis, MO) antibodies were used to identify macrophages and smooth muscle cells (SMCs), respectively. A subset of sections (n=48 from 8 arteries) were obtained by cryosectioning (5 μm thick) and staining with H&E and Oil Red O to identify lipid content. These were not included in the systematic analysis, but rather used to confirm findings from paraffin-embedded sections.

### Lesion Classification.

Each FLIm-IVUS image was equally divided into 12 sectors (Supplemental Figure 2G). Plaque morphology was assessed along the entire IVUS imaging depth and classified according to the modified morphologic classification system of the American Heart Association (2,14) as adaptive intimal thickening (AIT), intimal xanthoma (IX), pathologic intimal thickening (PIT), fibrous and fibrocalcific (F-FC), plaque rupture (PR), early fibroatheroma (EFA), late fibroatheroma (LFA), or thin-cap fibroatheroma (TCFA). See the Supplemental Methods section for details.

### Tabulation of Histologic Features.

For each sector, a list of histologic features was systematically evaluated. This assessment was performed over a depth of 200 μm from the luminal surface to match the expected FLIm penetration. Fibrous tissue types were classified as cellular fibrous, hypocellular dense fibrous, or loose fibrous. Cellular fibrous tissue was composed primarily of smooth muscle cells in a predominantly proteoglycan-rich extracellular matrix (ECM). Hypocellular fibrous tissue contained relatively low cellularity, often with dense collagen. Loose fibrous tissue had variable cellularity, with an arrangement of relatively thinner collagen fibrils. Movat's pentachrome staining was used to broadly assess ECM composition, which was qualitatively categorized as predominantly collagen rich, proteoglycan rich, a collagen and proteoglycan admixture, or containing extracellular lipid (ECL). Grading of smooth muscle cells (identified by α-SMA immunostaining) and mFC cellularity (identified by CD68 staining) was performed by using semiquantitative scales, as detailed in the Supplemental Methods. Medial smooth muscle cells percentage, calcification, hemorrhage, and necrotic core were recorded as a percentage (0–100%) of the region of interest. For calcification, proximity to the lumen was recorded as superficial, within 100 μm, within 200 μm, or beyond 200 μm. The internal elastic lamina was recorded as present or absent within the region of interest. Most CD68+ cells in the coronary arteries are mFCs and, thus, are referred to as such unless noted otherwise.

### Coregistered Histology and Imaging Dataset.

Each histologic ring was matched to its respective IVUS image. This coregistration was performed on the basis of pullback distance information, anatomic landmarks (eg, arterial branches or calcification patterns), and luminal shape (Supplemental Figure 4). For each section of the imaging dataset, the arc of each angular sector was adjusted to account for tissue deformation during the fixation process. For each sector, individual FLIm measurements (ie, pixel) were associated with the tabulated histology values from that sector. The study database consisted of 33,980 pixels from 2448 locations (30° arc) obtained from 204 sections of 32 artery segments.

### Statistical and Machine Learning Methods.

A Shapiro-Wilk test showed that FLIm-derived parameters were not normally distributed. Therefore, the sector-averaged FLIm parameters associated with histologic features were evaluated for statistically significant variations by using a Kruskal-Wallis test with a Mann-Whitney U test for pairwise comparisons. No adjustments were made for correlated observations within individuals. We used a piecewise linear regression model based on 540-nm lifetime to quantify mFC presence. The model was evaluated by a leave-one-out cross-validation approach, whereby a full artery segment was removed for each fold. The consistency of the model across folds was assessed by reporting the coefficients of the linear piecewise linear regression obtained for each fold (Supplemental Figure 5). We evaluated the ability to detect inflammation by computing the receiver operator characteristic (ROC) curve for the pixel-level identification of non-inflamed and inflamed locations (<10%: mFC scores 0–1 vs. >10%: mFC score 2–4) and of non-inflamed and highly inflamed locations (<10%: mFC scores 0–1 vs. >10%: mFC score 3–4). ROC curves were calculated by comparing the true positive rate and false positive rate of point measurements to identify the effect of varying predictor output cut-off threshold values. An ROC analysis was also performed on the detection of superficial calcification. The output of the classifier was displayed as a 3D rendering of the mFC score, with FLIm-IVUS cross sections and corresponding CD68-stained histology sections.

## RESULTS

We performed univariate analysis to compare FLIm parameters (averaged within each section) with the associated tissue characteristics identified on histologic analysis. No adjustments were made for correlations that may exist between observations within each coronary segment; thus, the reported p-values may overestimate the differences in FLIm signature between different lesions phenotypes and compositions. Results for select FLIm parameters by lesion type, ECM composition, and mFC are presented below. Comprehensive results from the univariate analysis, including the number of samples and sectors for each group, are shown in Supplemental Figures 6–12.

### Lesion Type.

Normal arteries showed the shortest lifetimes in the 390-nm and 540-nm bands (Figure 1). The first group of lesions (ie, AIT, F-FC, IX) showed slightly prolonged 390-nm lifetimes, whereas the remainder of the lesions (ie, PIT, EFA, LFA, TCFA, PR) showed the longest 390-nm lifetimes. A somewhat different picture was seen for 540-nm lifetimes. Normal, AIT, and F-FC lesions showed the shortest lifetimes, whereas PIT, IX, PR, EFA, and LFA lesions showed longer lifetimes with wide distributions, and the TCFA lifetime was consistently long. Some of the features used to determine lesion type (deeper lipid pools, calcifications, necrotic core) are beyond the penetration depth of FLIm, leading to the overlap of FLIm signatures observed for various plaque subtypes.

### ECM Composition and Superficial Calcification.

The 390-nm and 450-nm bands' lifetime distributions for each tabulated ECM composition (Figure 1B, see Supplemental Figure 10 for all spectral bands) illustrate that the presence of

ECL in the matrix was associated with longer lifetimes (P<0.0001). In locations of longer 390-nm lifetime (Figure 2), ECL was absent within the FLIm penetration depth; thus, ECL was not the direct cause of the observed FLIm contrast. This finding was corroborated by the wide distribution of 390-nm lifetimes observed in collagen and collagen-proteoglycan–rich lesions (Figure 1B), confirming that ECL was not causing the observed 390-nm contrast, although prolonged lifetime was most prevalent in lesions where deeper ECL accumulation was present, such as PIT, FA, and PR (Figure 2I). Focusing on the fibrous type classification (Supplemental Figure 7), we found that prolonged 390-nm lifetime was most prevalent in superficial cellular layers of complex lesions and loose fibrous areas, both typically associated with newly formed tissue (15), as shown in Figure 2J–K. Finally, the presence of superficial calcium was associated to a shorter 450-nm lifetime than all other compositions (P<0.0001) (Figure 1B). Fibrocalcific lesions where calcifications abutted the lumen showed a markedly reduced 450-nm lifetime signature (ROC-AUC=0.90, Figure 3).

### mFC Cellularity Score and Lipid Content.

Locations characterized by higher mFC scores were associated with a significantly prolonged 540-nm band lifetime (P<0.0001), except for locations with scores 3 and 4 (Figures 1A and 4, and Supplemental Figure 14). In contrast, at 390 nm, only score 0 was significantly different from the higher scores. This result is consistent with the longer 540-nm lifetime reported for PIT, EFA/LFA/TCFA, and PR, which are characterized by high levels of mFCs. Locations associated with extracellular lipid, in the absence of mFC infiltration, only showed a slightly higher 540-nm lifetime (+18%) (Figure 4K–M). A site containing epicardial adipose tissue showed a similarly extended lifetime, suggesting that a FLIm signal at 540 nm is highly sensitive to intracellular oxidized lipid content. Hemosiderin-rich macrophage clusters led to a short 540-nm lifetime (Supplemental Figure 13B–C), making them easily differentiated from the more typical lipid-laden mFCs present at separate locations within the same artery.

### mFC Predictor.

Figure 5 shows the agreement between mFC ratings predicted from 540-nm band lifetime and the mFC content as assessed by CD68-staining on histologic sections. For all samples studied, the predictor showed good agreement with mFC histologic scoring performed by the pathologist (r=0.52; Figure 5J). For reference, a comparison of mFC scoring for select locations between 2 pathologists showed a correlation coefficient of 0.83 (Figure 5K). Supplemental Figure 14 shows another case study of mFC score prediction. The ROC curve analysis shows the ability to discriminate between inflamed (>10% mFC area) and non-inflamed locations (>10% mFC area) by 540-nm lifetime (ROC-AUC: 0.86, Figure 5L). Focusing on highly inflamed locations (>25% mFC area) further improved discrimination (ROC-AUC: 0.94).

## DISCUSSION

In this study, we systematically examined the relationship between FLIm-derived parameters and the biochemical makeup of distinct pathologic features of arterial lesions. Our findings indicate that parameters from 3 spectral bands can be used to detect superficial calcium,

quantitatively predict the presence of mFCs in the luminal layers, and possibly detect recent plaque accumulation. Importantly, this study was performed with a FLIm-IVUS catheter system suitable for in vivo imaging of coronary arteries (10), indicating that FLIm technology is ready for clinical translation.

### Imaging validation approach.

To our knowledge, this is the first reported comprehensive evaluation of FLIm imaging data at the pixel level. We utilized the rich spatial variations of the FLIm signature over the intimal surface and performed a systematic assessment of biochemical and histologic features that captures the heterogeneous distribution of plaque constituents. In contrast to previous fluorescence lifetime–based studies of the coronary arteries that were limited to well-defined lesions (6–8), our study integrated all luminal regions of each arterial ring so that the FLIm signature could be evaluated with respect to varying levels of constituents in the arterial wall. Because of the limited penetration of ultraviolet light into tissue, FLIm imaging provides information about the superficial layers of the lesions (ie, “sectioning”) thought to be highly relevant in the pathophysiology of atherosclerotic lesions.

The fine coregistration of the imaging data with histology sections, using IVUS to provide morphologic information (branches, calcifications, lumen shape), is paramount for performing a robust evaluation of the correspondence between the FLIm signature and histologic features. During this fine registration process, the FLIm information was withheld, avoiding the introduction of possible bias into the study.

### Use of FLIm Parameters in the Red-shifted Wavelengths (540-nm band) for the Prediction of Superficial mFC Infiltration.

The infiltration of macrophages and their subsequent conversion into mFCs marks an inflammatory process that plays a critical role in both the progression and destabilization of atherosclerotic lesions (16). The early retention of matrix-bound lipoproteins (14,17,18) causes trafficking macrophages to internalize, metabolize, and accumulate a large amount of lipids. Initially, most lipids are stored as cholesteryl ester fatty acids (19); however, with time, the amount of peroxidized lipid–protein compounds increases. Some of these lipid compounds exhibit strong fluorescence emission upon ultraviolet excitation (4,5,20).

Although the idea that a link exists between intimal mFC accumulation and FLIm signatures was suggested previously (21), our results show for the first time that mFC presence is directly linked to changes in 540-nm lifetime. We showed that increased 540-nm lifetimes were strongly correlated with increased levels of mFC infiltration, allowing the creation of a predictor that can map the location and degree of mFC infiltration over the vessel lumen surface with high accuracy. This method compares favorably with the identification of macrophages by intravascular optical coherence tomography, which requires image processing by expert readers in a core laboratory (22) and is subject to artifacts (23). This wavelength range does not correspond to the fluorescence emission of all pure forms of lipids, but it has been linked with the fluorescence emission properties of the peroxidized lipids–proteins complex ceroid (4,20), which are byproducts of the uptake and oxidation of low-density lipoprotein by macrophages (20,24,25). Poor degradation of oxidized low-

density lipoprotein leads to their accumulation in foam cells, which are associated with cell injury and necrosis (20). In addition, a cytotoxicity effect was shown in vitro, which may lead to lesion irreversibility by the formation of a “death zone” (26). Future studies are warranted to establish the link between peroxidized lipids content and lesion progression. We also determined that accumulation of iron-rich macrophages led to a similar red-shifted emission but a short lifetime, suggesting that these macrophages could potentially be differentiated from lipid-rich mFCs.

### Potential Use of FLIm Parameters in the Blue-shifted Wavelengths (390-nm band) to Highlight New Plaque Accumulation.

We observed strong variations in lifetime values across the luminal surface, which were lowest for healthy and fibrous or fibrocalcific regions and highest for PIT, fibroatheroma, and PR. Initially, this may suggest an association with ECL, but no histological evidence of ECL presence within the penetration depth of FLIm could be found in many locations of increased 390-nm lifetime (Figure 2E, G). This finding is reflected in the wide 390-nm lifetime distribution observed in collagen- and proteoglycan-rich superficial layers lacking superficial ECL (Figure 1B).

Because the increase was observed in PIT lesions (considered to be early progression-prone entities) (27) and healed thrombus in complex layered plaques, 390-nm lifetime contrast may indicate areas of active plaque growth. If confirmed, this finding would be of great clinical significance.

The spectral overlap of various fluorescent biochemical species (ie, lipids, elastin, collagen, proteoglycans) (4) in this wavelength range and the colocalization of lipids and proteoglycans as described in the early retention hypothesis (14,17,18) prevented the unambiguous association of lifetime changes with the abundance of a particular species. Our results indicate that the concurrent lifetime and spectral ratio increases in the blue-shifted spectral range point to the contribution of a single fluorophore (Supplemental Figure 15). Identifying this fluorophore could be the objective of future studies.

### Complementarity with existing intravascular imaging techniques.

We showed that FLIm can reliably quantify superficial inflammation and provide information about ECM composition, which existing intravascular imaging modalities cannot do. These FLIm-derived data are complementary to compositional information derived from existing intravascular imaging techniques. For example, radiofrequency analysis of the IVUS backscatter signal (IVUS-VH) can detect necrotic cores but has no sensitivity to plaque inflammation and lacks the spatial resolution to provide information about a plaque’s intimal surface. Near-infrared spectroscopy has a well-documented ability to detect lipid-core plaques but is not sensitive to inflammation and cannot differentiate between superficial and deeper accumulations. Optical coherence tomography provides exquisite high-resolution images of a plaque’s morphology, but whether it can reliably identify macrophages is unclear (28).

### Study Limitations.

Univariate comparison was performed without adjustments for correlated observations within each sample, thus the p-values reported here may be underestimated. To compensate for this limitation, the univariate analysis findings were corroborated with ROC analysis performed using a leave-one-sample-out approach that is not affected by the dependence between multiple observations for the same artery segment. Our findings in ex vivo specimens require validation in vivo to confirm that similar contrast can be observed. The source of the 390-nm band signaling could not be elucidated from histological findings alone and will require further investigation by additional methodologies. Furthermore, confirming this wavelength as a marker of active plaque growth may require multi–time-point in vivo studies.

## Conclusion

Intravascular spectroscopy with the use of FLIm provides valuable information for characterizing atherosclerotic lesions in coronary arteries. More specifically, FLIm supports the identification of atherosclerotic plaque of various morphologies, from early progression-prone lesions to advanced ones, and the quantification of inflammatory activity. This information improves our understanding of plaque development and may ultimately be used to improve risk assessment in patients at risk of acute coronary events.

## Supplementary Material

Refer to Web version on PubMed Central for supplementary material.

## Acknowledgment:

The Department of Scientific Publications of the Texas Heart Institute provided editorial support.

**Sources of funding:** This work was supported by NIH grants R01-HL67377 (to LM) and R01-HL105993 (to KBM).

## ABBREVIATIONS AND ACRONYMS

| | |
|---|---|
| **AIT** | adaptive intimal thickening |
| **ECL** | extracellular lipid |
| **ECM** | extracellular matrix |
| **EFA** | early fibroatheroma |
| **F-FC** | fibrous-fibrocalcific |
| **FLIm** | fluorescence lifetime imaging |
| **IVUS** | intravascular ultrasonography |
| **IX** | intimal xanthoma |
| **LFA** | late fibroatheroma |

| | |
|---|---|
| **PIT** | pathological intimal thickening |
| **PR** | plaque rupture |
| **TCFA** | thin-cap fibroatheroma |

## REFERENCES


1. Insull W Jr, The pathology of atherosclerosis: plaque development and plaque responses to medical treatment. Am J Med2009;122:S3–S14.
2. Virmani R, Kolodgie FD, Burke AP, Farb A, Schwartz SM, Lessons from sudden coronary death. Arterioscler Thromb Vasc Biol2000;20:1262–75. [PubMed: 10807742]
3. Michail M, Serruys PW, Stettler R, et al., Intravascular multimodality imaging: feasibility and role in the evaluation of coronary plaque pathology. Eur Hear J - Cardiovasc Imaging2017;18:613–20.
4. Croce AC, Bottiroli G, Autofluorescence spectroscopy and imaging: a tool for biomedical research and diagnosis. Eur J Histochem2014;58:2461. [PubMed: 25578980]
5. Marcu L, Fishbein MC, Maarek J-MI, Grundfest WS, Discrimination of human coronary artery atherosclerotic lipid-rich lesions by time-resolved laser-induced fluorescence spectroscopy. Arterioscler Thromb Vasc Biol2001;21:1244–50. [PubMed: 11451759]
6. Maarek J-MI, Marcu L, Fishbein MC, Grundfest WS, Time-resolved fluorescence of human aortic wall: use for improved identification of atherosclerotic lesions. Lasers Surg Med2000;27:241–54. [PubMed: 11013386]
7. Sun Y, Sun Y, Stephens D, et al., Dynamic tissue analysis using time- and wavelength-resolved fluorescence spectroscopy for atherosclerosis diagnosis. Opt Express2011;19:3890–901. [PubMed: 21369214]
8. Park J, Pande P, Shrestha S, Clubb F, Applegate BE, Jo JA, Biochemical characterization of atherosclerotic plaques by endogenous multispectral fluorescence lifetime imaging microscopy. Atherosclerosis2012;220:394–401. [PubMed: 22138141]
9. Fatakdawala H, Gorpas D, Bishop JW, et al., Fluorescence lifetime imaging combined with conventional intravascular ultrasound for enhanced assessment of atherosclerotic plaques: an ex vivo study in human coronary arteries. J Cardiovasc Transl Res2015;8:253–63. [PubMed: 25931307]
10. Bec J, Phipps JE, Gorpas D, et al., In vivo label-free structural and biochemical imaging of coronary arteries using an integrated ultrasound and multispectral fluorescence lifetime catheter system. Sci Rep2017;7:8960. [PubMed: 28827758]
11. Lee MW, Song JW, Kang WJ, et al., Comprehensive intravascular imaging of atherosclerotic plaque in vivo using optical coherence tomography and fluorescence lifetime imaging. Sci Rep2018;8:14561. [PubMed: 30267024]
12. Jo JA, Park J, Pande P, et al., Simultaneous morphological and biochemical endogenous optical imaging of atherosclerosis.Eur Hear J – Cardiovasc Imaging2015;16:910–8.
13. Liu J, Sun Y, Qi J, Marcu L, A novel method for fast and robust estimation of fluorescence decay dynamics using constrained least-squares deconvolution with laguerre expansion. Phys Med Biol2012;57:843. [PubMed: 22290334]
14. Nakagawa K, Nakashima Y, Pathologic intimal thickening in human atherosclerosis is formed by extracellular accumulation of plasma-derived lipids and dispersion of intimal smooth muscle cells. Atherosclerosis2018;274:235–42. [PubMed: 29622338]
15. Bentzon JF, Otsuka F, Virmani R, Falk E, Mechanisms of plaque formation and rupture. Circ Res2014;114:1852. [PubMed: 24902970]
16. Gonzalez L, Trigatti BL, Macrophage apoptosis and necrotic core development in atherosclerosis: a rapidly advancing field with clinical relevance to imaging and therapy. Can J Cardiol2017;33:303–12. [PubMed: 28232016]
17. Nakashima Y, Fujii H, Sumiyoshi S, Wight TN, Sueishi K, Early human atherosclerosis: accumulation of lipid and proteoglycans in intimal thickenings followed by macrophage infiltration. Arterioscler Thromb Vasc Biol2007;27:1159–65. [PubMed: 17303781]

18. Otsuka F, Kramer MCA, Woudstra P, et al., Natural progression of atherosclerosis from pathologic intimal thickening to late fibroatheroma in human coronary arteries: a pathology study. Atherosclerosis2015;241:772–82. [PubMed: 26058741]
19. Tabas I, Cholesterol and phospholipid metabolism in macrophages.Biochim Biophys Acta - Mol Cell Biol Lipids2000;1529:164–74.
20. Haka AS, Kramer JR, Dasari RR, Fitzmaurice M, Mechanism of ceroid formation in atherosclerotic plaque: in situ studies using a combination of raman and fluorescence spectroscopy. J Biomed Opt2011;16:11011–7.
21. Marcu L, Jo JA, Fang Q, et al., Detection of rupture-prone atherosclerotic plaques by time-resolved laser-induced fluorescence spectroscopy. Atherosclerosis2009;204:156–64. [PubMed: 18926540]
22. Taguchi Y, Itoh T, Oda H, et al., Coronary risk factors associated with oct macrophage images and their response after cocr everolimus-eluting stent implantation in patients with stable coronary artery disease. Atherosclerosis2017;265:117–23. [PubMed: 28881269]
23. Phipps JE, Vela D, Hoyt T, et al., Macrophages and intravascular oct bright spots: a quantitative study. JACC Cardiovasc Imaging2015;8:63–72. [PubMed: 25499133]
24. Hoppe G, Ravandi A, Herrera D, Kuksis A, Hoff HF, Oxidation products of cholesteryl linoleate are resistant to hydrolysis in macrophages, form complexes with proteins, and are present in human atherosclerotic lesions. J Lipid Res1997;38:1347–60. [PubMed: 9254061]
25. Wen Y, Leake DS, Low density lipoprotein undergoes oxidation within lysosomes in cells. Circ Res2007;100:1337–43. [PubMed: 17446432]
26. Li W, Östblom M, Xu L, et al., Cytocidal effects of atheromatous plaque components: the death zone revisited. FASEB J2006;20:2281–90. [PubMed: 17077305]
27. Kolodgie FD, Burke AP, Nakazawa G, Virmani R, Is pathologic intimal thickening the key to understanding early plaque progression in human atherosclerotic disease?Arterioscler Thromb Vasc Biol2007;27:986–9. [PubMed: 17442894]
28. Ramasamy A, Serruys PW, Jones DA, Reliable in vivo intravascular imaging plaque characterization: a challenge unmet. Am Heart J2019;218.

## Perspectives

**COMPETENCY IN MEDICAL KNOWLEDGE:**

The autofluorescence signature of the arterial wall is modified by the presence of different constituents, which can be identified from their lifetime and spectral properties. Superficial macrophage foam cells generate a strong lifetime increase in the red-shifted wavelengths, whereas matrix components associated with superficial calcification and recent plaque formation are identified in the blue and near-ultraviolet wavelengths.

**TRANSLATIONAL OUTLOOK:**

Fluorescence lifetime is ready for clinical translation, and future work will focus on the design, manufacturing, and regulatory activities required to support clinical studies with intravascular FLIm. These studies are needed to confirm during percutaneous coronary intervention that the FLIm contrast observed in ex vivo coronary samples is also present in patients. Additionally, confirmation that newly formed lesion can be identified with FLIm may require multi–time-point studies.

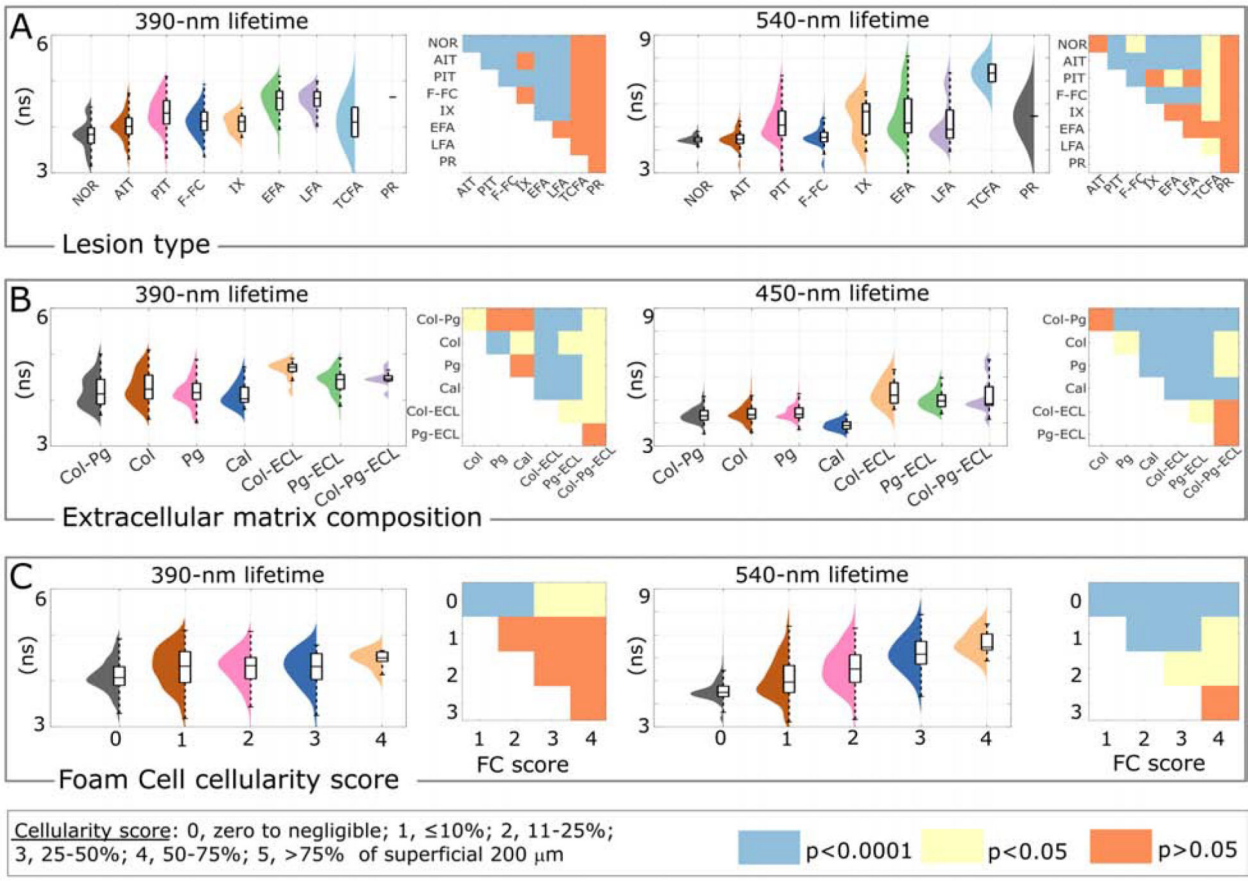


**Figure 1. Evaluation of fluorescence lifetime imaging (FLIm) signatures for select histologic compositions.**

FLIm signals are shown at multiple wavelength bands for select histologic features. Pairwise comparisons were performed on the averaged FLIm parameters for each 30° sector by using a Mann-Whitney U test to compare the differences between groups ($P<0.0001$) and are displayed in matrix form. No adjustments were made for correlated observations within artery segments. (**A**) 390-nm band: Normal (NOR) locations show the shortest lifetime. Pathologic intimal thickening [PIT], plaque rupture [PR], early/late fibroatheroma [EFA/LFA], and thin-cap fibroatheroma [TCFA] show the highest lifetimes. 540-nm band: Adaptive intimal thickening (AIT), and fibrous and fibrocalcific (F-FC) regions show the shortest lifetimes. TCFA locations show long 540-nm lifetimes. Other lesion types show wider distributions of lifetimes. (**B**) Extracellular matrix (ECM) composition was evaluated based on the presence of collagen (Col), proteoglycan (Pg), extracellular lipid (ECL), and calcification (Cal; 100% at lumen). Fibrotic regions (which are Col-Pg rich) present shorter 390-nm and 450-nm lifetimes than lipid–rich regions. The presence of superficial calcification was linked to a significantly decreased 450-nm lifetime. (**C**) Locations with increased macrophage foam cell (mFC) scores show an increased average lifetime in the 540-nm band but little lifetime variation in the 390-nm band.

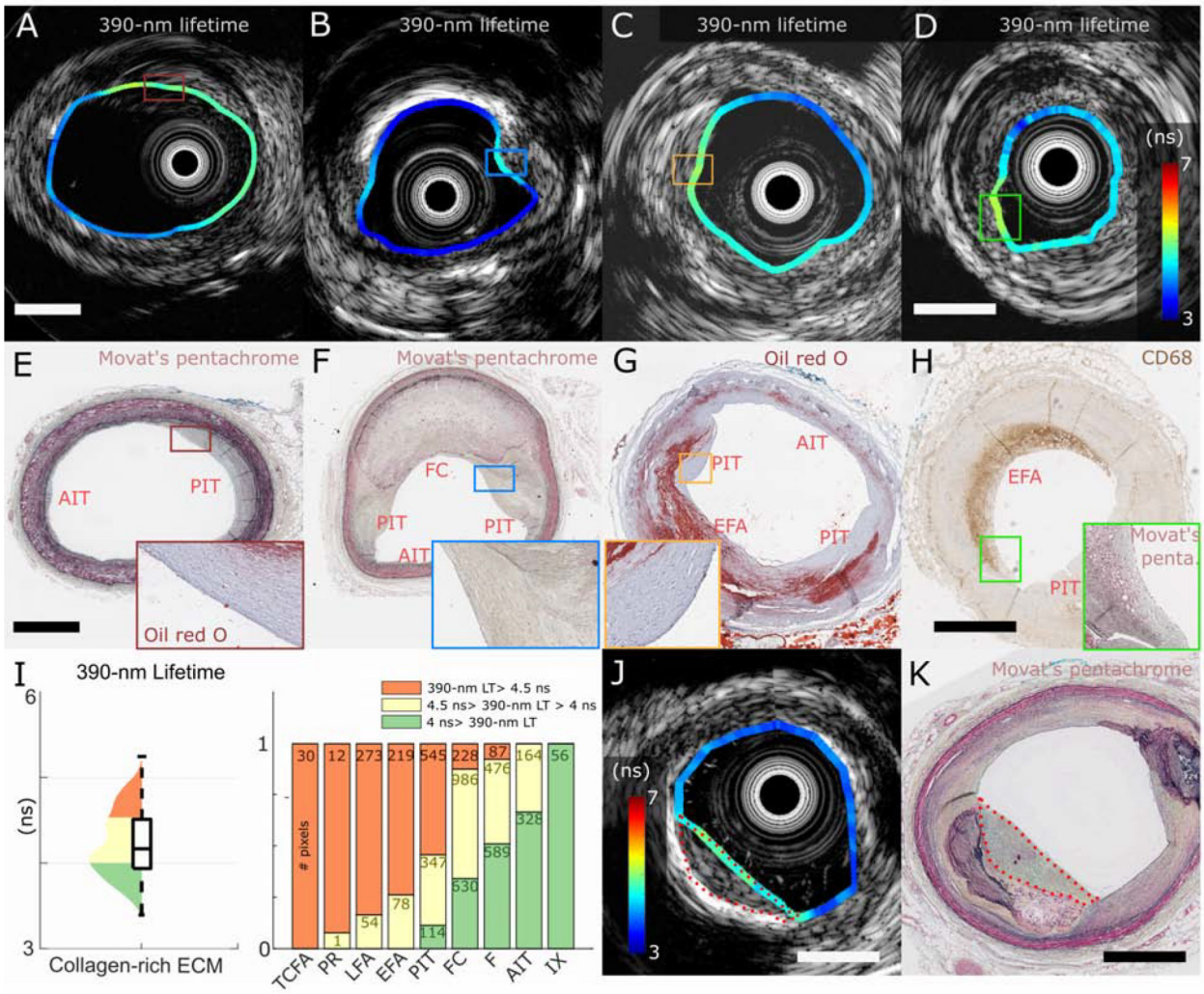


**Figure 2. Increased 390-nm lifetime values in progressing lesions.**

(**A, B, C, E, F, G**) Pathologic intimal thickening (PIT) lesions show greater 390-nm lifetime values than healthier adaptive intimal thickening (AIT) or solid fibrocalcific (FC) lesions. The absence of oil red O staining within the FLIm penetration depth (~200 μm) in some lesions indicates that the contrast is not caused by extracellular lipids. (**I**) For collagen-rich extracellular matrix (ECM) locations (without ECL at the intimal surface), longer 390-nm lifetimes are associated with ECL-rich lesion types. Thus, these lesions may also show superficial compositional changes to which FLIm is sensitive. (**D**, **H**) The early fibroatheroma (EFA) region shows that the strong presence of macrophage foam cells (intracellular lipids) does not lengthen 390-nm lifetimes. (**J,K**) In multilayered lesions, newly incorporated (superficial) layers often show prolonged 390-nm lifetime, suggesting a link between 390-nm contrast and active plaque growth. F: fibrous tissue; FC: fibrocalcific; LFA: late fibroatheroma; IX: intimal xanthoma; PR: plaque rupture; TCFA: thin-cap fibroatheroma. Scale bar=1 mm.

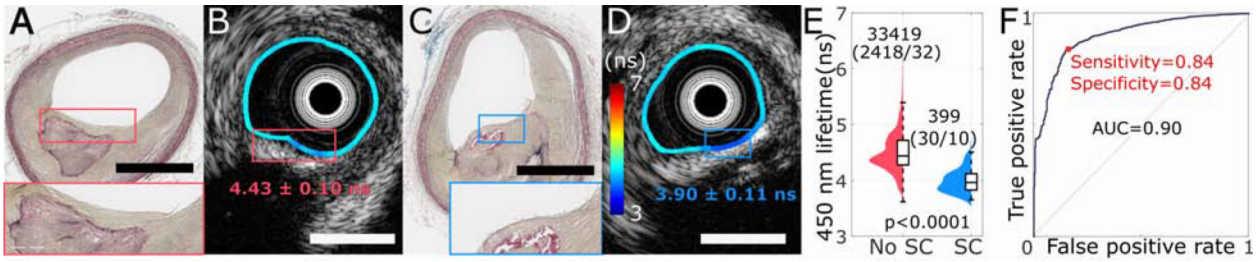


**Figure 3. Contrast of fluorescence lifetime imaging (FLIm) signal at 450 nm consistent with the presence of superficial calcium.**

(**A,C**) Movat's pentachrome–stained section of fibrocalcific plaques with a thin fibrous layer between calcium and the lumen (red box) and calcium at the lumen (blue box). (**B,D**) Corresponding FLIm–IVUS images depict that shorter lifetime is present only in areas with superficial calcium. (**E**) Regions with calcification at the lumen (blue) present shorter lifetime values at 460 nm than regions without superficial calcium (red). The number of FLIm pixels (number of locations/number of subjects) is specified for each group. (**F**) ROC curve computed for the pixel-level identification of superficial calcium indicates robust identification of these locations. Scale bar=1 mm.

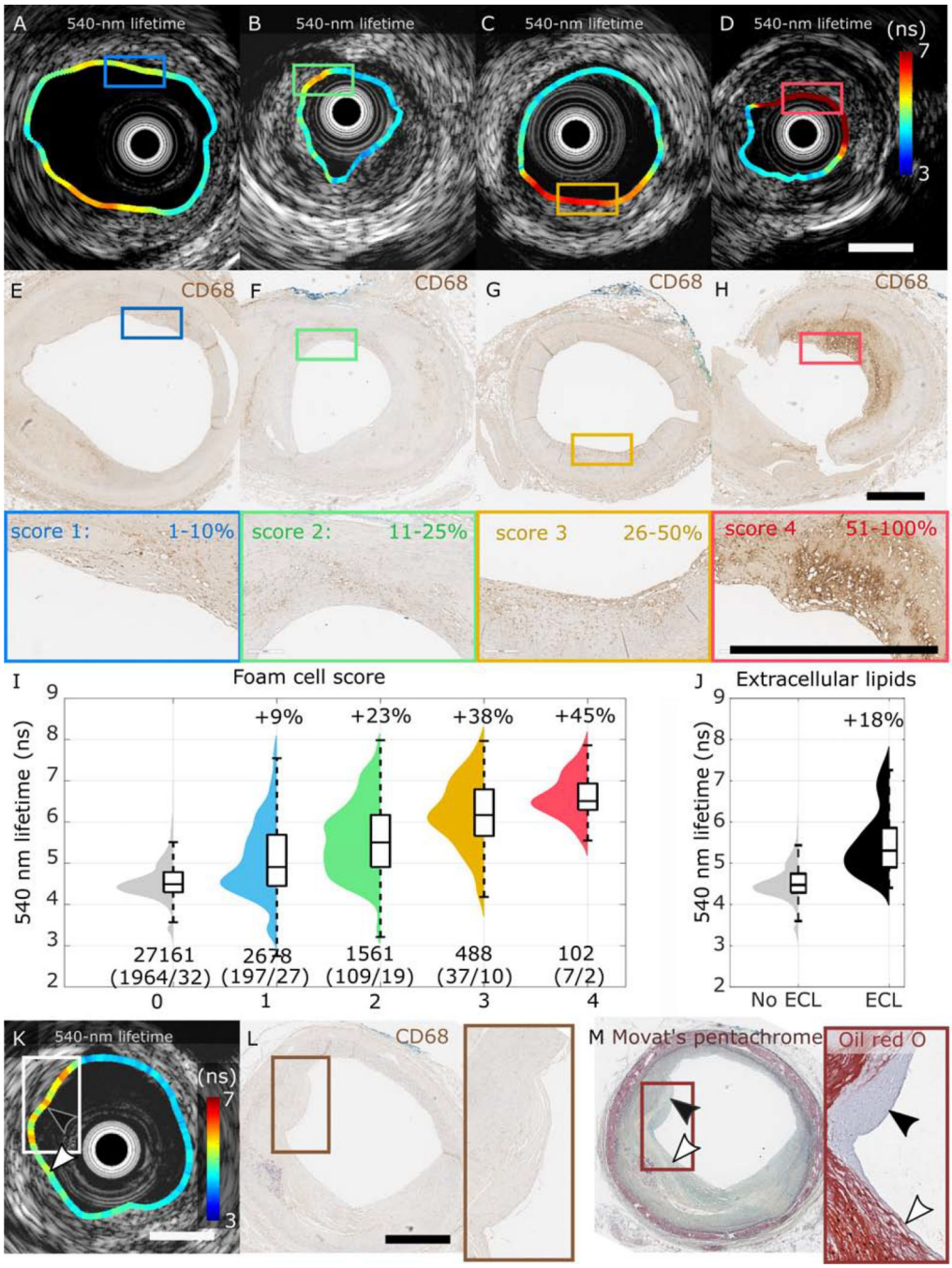


**Figure 4. Correlation of fluorescence lifetime imaging (FLIm) signal at 540 nm with macrophage foam cell (mFC) infiltration.**

(**A-D**) Representative 540 nm FLIm–intravascular ultrasonography (IVUS) images illustrating increasing mFC scores. (**E-H**) Corresponding histology sections. (**I**) Lifetime histogram representing each mFC score in the dataset. The number of FLIm pixels (number of locations/number of subjects) for each mFC score is specified. (**J**) The presence of extracellular lipid (ECL) in the absence of mFCs led to moderately increased 540-nm lifetimes (+15%). The FLIm-IVUS images at 540 nm show increased lifetimes in the 4$^{th}$

quadrant (black arrowhead) (**K**). This location has mFCs in the CD68 section (**L**) but no superficial lipids in the Oil Red O section (**M**). In contrast, the 3rd quadrant (white arrowhead) presents superficial lipids but no mFCs and shows a limited increase in lifetime, illustrating that mFCs, independent from lipids, generate lifetime contrast. Scale bar=1 mm.

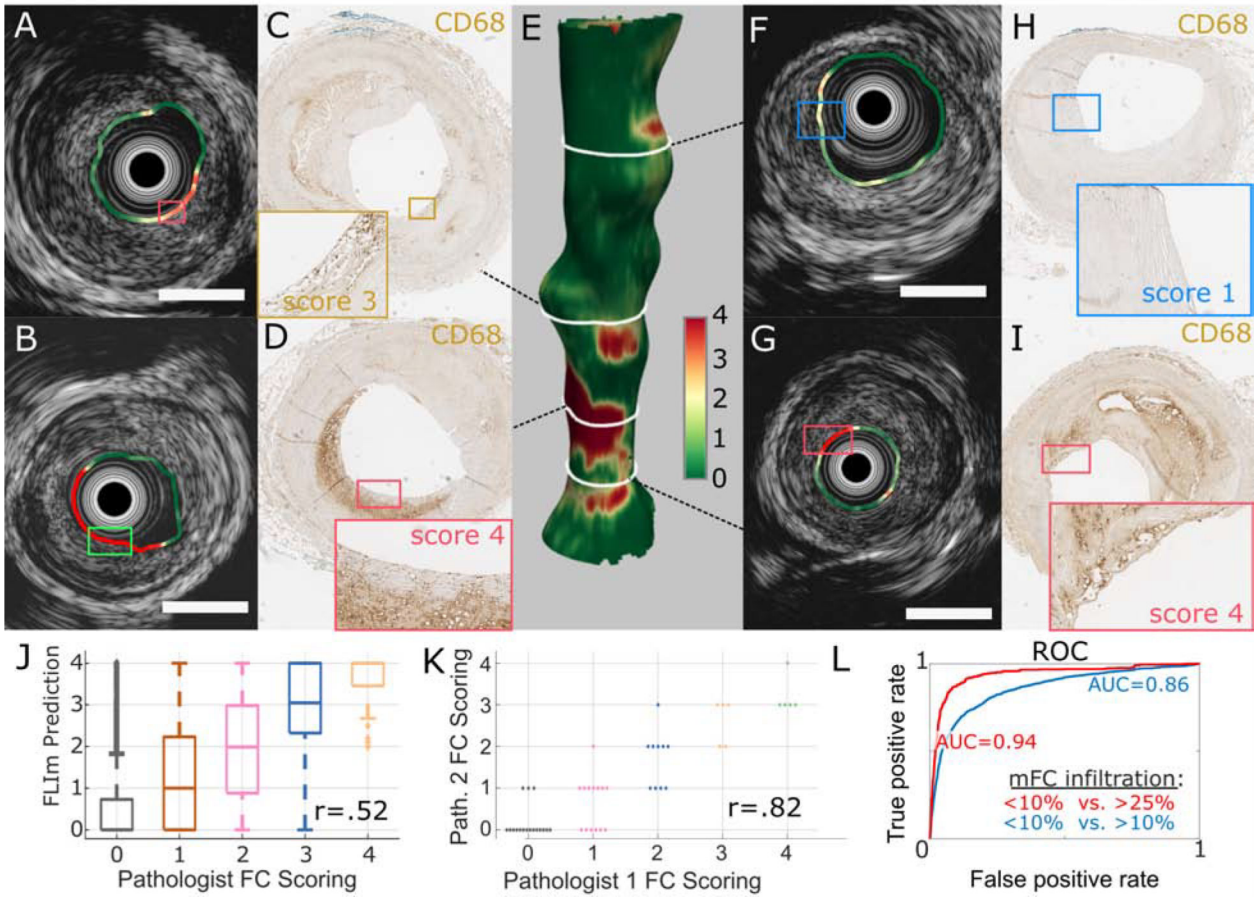


**Figure 5. Case study of macrophage foam cell (mFC) prediction rendered in 3D.**

(**A**) 3D rendering of the artery's luminal surface with the predictor rating. Four locations (**B, C, F, G**) for which histology was tabulated (**D, E, H, I**) are shown. For each section, the predicted distribution of mFCs closely matched the histologic findings. (**J**) Comparison of the predictor, derived from the 540-nm lifetime, with the pathologist-rated mFC scores. (**K**) Comparison of interobserver readings (pathologist 1 vs. pathologist 2) to evaluate the repeatability of mFC scoring by expert readers. (**K**) ROC curves computed for the pixel-level identification of FC infiltration (<10% vs. >10%, <10% vs. >25%) indicate robust identification of these locations.

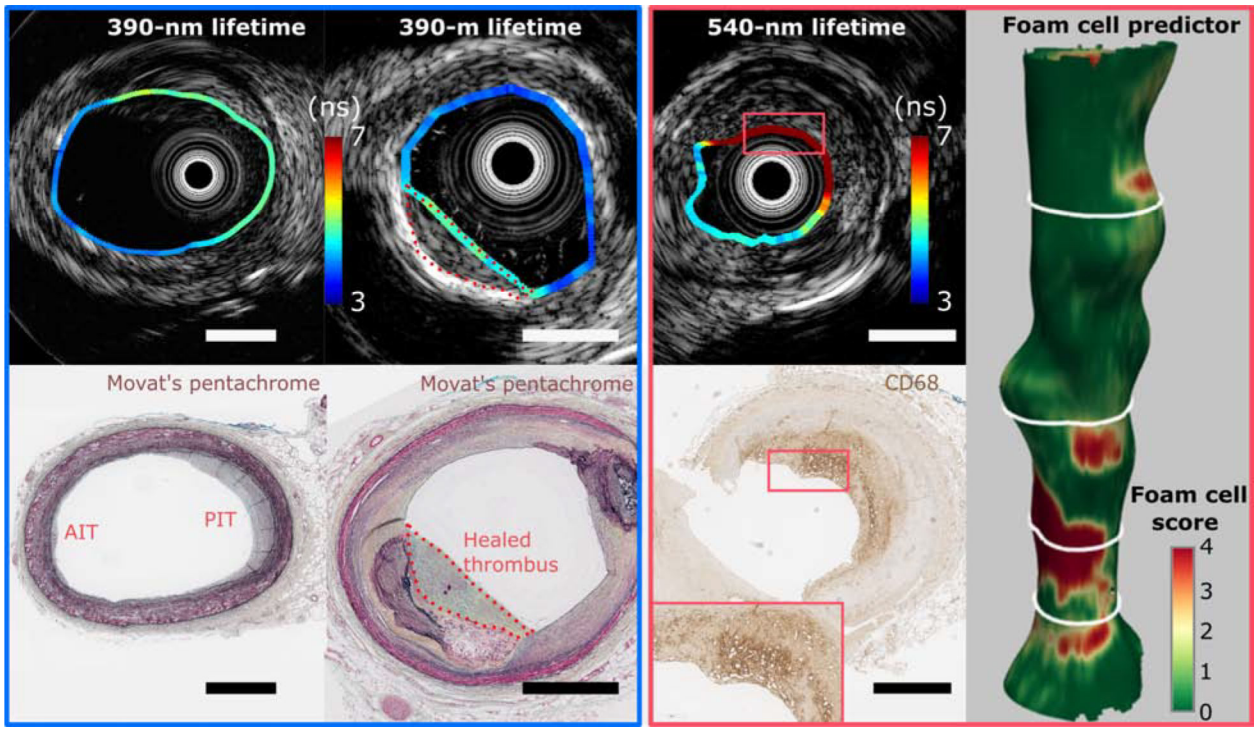


**Central Illustration. Plaque characterization with IV-FLIm**

Intravascular fluorescence lifetime enables label-free identification of lesions consistent with new plaque formation (390-nm band, left) and quantification and prediction of superficial macrophage foam cell infiltration (540-nm band, right)